Geophysical Prospecting, 1996, 44, 99–129

Full frequency-range transient solution for compressional waves in a fluid-saturated viscoacoustic porous medium[1]

José M. Carcione[2] and Gerardo Quiroga-Goode[2]

Abstract

An analytical transient solution is obtained for propagation of compressional waves in a homogeneous porous dissipative medium. The solution, based on a generalization of Biot's poroelastic equations, holds for the low- and high-frequency ranges, and includes viscoelastic phenomena of a very general nature, besides the Biot relaxation mechanism. The viscodynamic operator is used to model the dynamic behaviour associated with the relative motion of the fluid in the pores at all frequency ranges. Viscoelasticity is introduced through the standard linear solid which allows the modelling of a general relaxation spectrum. The solution is used to study the influence of the material properties, such as bulk moduli, porosity, viscosity, permeability and intrinsic attenuation, on the kinematic and dynamic characteristics of the two compressional waves supported by the medium. We also obtain snapshots of the static mode arising from the diffusive behaviour of the slow wave at low frequencies.

Introduction

The acoustics of porous media, within the framework of petroleum geophysics, have been receiving more attention in recent years. Regional exploration seismology aimed at the discovery of hydrocarbon reservoirs is based on simplified rheological models and ray representations of the wavefield. In the past, these approximations were sufficient, since the degree of resolution required was not high. In the present time, when most reservoirs are delimited, the need to increase the resolution and use not only the traveltimes but also the information contained in the amplitude and phase of the seismic wavefield has gradually emerged. The new exploration scenario is confined to reservoir areas and involves the presence of oil wells and data from seismic logs and well seismics, which have enough resolution to 'see' the effects of bulk properties, porosity, permeability, fluid content and fluid–solid interaction on the seismic pulse. In this case, the correct

[1] Paper presented at the 56th EAEG meeting, June 1994, Vienna. Received May 1994, revision accepted April 1995.

[2] Osservatorio Geofisico Sperimentale, PO Box 2011, Opicina, 34016 Trieste, Italy.

description of the reservoir response requires the modelling of reservoir rocks by porous media and the use of the full wavefield solution (e.g. Lumley *et al.* 1994).

Biot (1956a, b, c, 1962a, b) developed a theory of propagation of elastic waves in porous media, where the two-phase material is considered as a continuum, ignoring the microscopic level. Within this context, the macroscopic vriables follow the laws of continuum mechanics. Basically, the theory assumes that anelastic effects arise from viscous interactions between the fluid and the solid. The following assumptions are made in the theory.

1. The wavelength is large in comparison with the dimensions of the pores. This is a requirement for applying the theory of continuum mechanics, and implies that scattering dissipation is neglected.
2. Displacements are small, so that the macroscopic strain tensor is related to them by the nearest second-order approximation.
3. The liquid phase is continuous, such that pores are connected and the disconnected pores are part of the matrix frame.
4. Permeability is isotropic and the medium is fully saturated.

Biot demonstrated the existence of two kinds of compressional wave in a porous medium: the fast wave for which the solid and fluid displacements are in phase, and the slow wave for which the displacements are out of phase. At low frequencies, the medium does not support the slow wave, which becomes diffusive, since the fluid viscosity effects dominate (a thick boundary layer compared to the pore size). At high frequencies, tangential slip takes place (thin boundary layer), the inertial effects are predominant and the slow wave is activated. This wave contributes to the attenuation of the fast wave by mode conversion at inhomogeneities (Geerstma and Smit 1961; Turgut and Yamamoto 1988). Biot equations, in the low- and high-frequency ranges, were rederived by Auriault, Borne and Chambon (1985), by assuming a periodic pore structure from the microscopic level.

Transient solutions for propagation through ID fluid-saturated porous soils were obtained by Garg, Nayfey and Good (1974) and Sandhu, Shaw and Hong (1990). They obtained approximate analytical solutions by Laplace transfrom methods and finite-difference and finite-element techniques, respectively. In acoustics, Green's tensors for poroelastic media have been studied by Deresiewicz and Rice (1962), Burridge and Vargas (1979), Norris (1985) and Boutin, Bonnet and Bard (1987). The latter applied Auriault *et al.*'s (1985) theory to compute semi-analytical transient solutions in a stratified medium. Bonnet (1987) obtained a solution for the problem by applying the analogy between the poroelastic and thermoelastic equations, and Kazi-Aoual, Bonnet and Jouanna (1988) extended the solution of Boutin *et al.* (1987) to the transversely isotropic case. Most of these works give a detailed mathematical treatment of the problem but overlook the effects of the different material properties on the amplitude and phase of the wavefield. In fact, the Green's functions are rarely represented graphically and discussed. Modelling waves in porous media for geophysical prospecting is relatively recent: Has-

sanzadeh (1991), Zhu and McMechan (1991) and Dai, Vafidis and Kanasewich (1995) solved the 2D problem using finite-differences methods. In particular, Dai *et al.* (1995) compared their results with analytical solutions for the poroelastic case neglecting the Biot mechanism.

However, it is well known that the attenuation values predicted by Biot theory are much smaller than those measured experimentally (Mochizuki 1982). In fact, Biot (1962a) states that the model of a purely elastic matrix saturated with a viscous fluid is only applicable in exceptional cases. Hence, he generalizes the theory to general dissipation by using the correspondence principle, in this way including solid and fluid attenuations, dissipation due to non-connected pores (they are part of the solid), etc. Similarly, the theory can model other more complex mechanisms, such as thermoelastic dissipation, which produce a relaxation spectrum, or local flow mechanisms like the 'squirt' flow involving motion of the fluid between the grains (Murphy, Winkler and Kleinberg 1986; Dvorkin, Nolen-Hoeksema and Nur 1994). A time-domain formulation based on memory (hidden) variables is given by Carcione (1993); this time-domain wave equation (with relaxation times) accounts for the levels of attenuation observed experimentally in porous rocks.

Biot (1962b) introduced the viscodynamic operator to account for the dynamic properties of the fluid motion in the pores, valid in both the low- and high-frequency ranges. This operator is the sum of a viscosity term (static Darcy's law) plus an inertial term. At low frequencies, the fluid flow is of the Poiseuille type and the inertia forces are negligible in comparison with the effects of the viscosity. At high frequencies these effects are confined to a thin boundary layer in the vicinity of the solid and the inertia forces are predominant. Auriault *et al.* (1985) rederived the viscodynamic operator from the microscopic level. They refer to this operator as the generalized Darcy coefficient.

Within this framework, we obtain an analytical transient solution for propagation of compressional waves in a homogeneous saturated porous medium, where anelasticity is modelled by standard linear solid elements representing different dissipation mechanisms. The paper is organized as follows. The first section introduces the constitutive law and the field equations. Then, we obtain the 2D and 3D frequency-domain solutions in closed form. Next, we illustrate how to introduce intrinsic dissipation in a realistic way and give the expressions for the phase velocities and attenuations of the compressional waves. Finally, we analyse the 3D transient response as a function of the material parameters, frequency range, intrinsic dissipation, space dimensions and type of source.

Field equations

The frequency-domain stress–strain relationships for a linear viscoelastic, isotropic porous solid (Biot 1962a, b) are

$$\sigma_{xx} = He - 2\mu(\varepsilon_{yy} + \varepsilon_{zz}) - C\zeta, \tag{1}$$

$$\sigma_{yy} = He - 2\mu(\varepsilon_{xx} + \varepsilon_{zz}) - C\zeta, \tag{2}$$

$$\sigma_{zz} = He - 2\mu(\varepsilon_{xx} + \varepsilon_{yy}) - C\zeta, \tag{3}$$

$$\sigma_{yz} = 2\mu\varepsilon_{yz}, \tag{4}$$

$$\sigma_{xz} = 2\mu\varepsilon_{xz}, \tag{5}$$

$$\sigma_{xy} = 2\mu\varepsilon_{xy}, \tag{6}$$

and

$$p_f = -Ce + M\zeta, \tag{7}$$

where σ_{ij} are the stress components of the bulk material, ε_{ij} are the strain components of the solid matrix, e and ζ are the dilatations of the solid and of the fluid relative to the solid, respectively, and p_f is the fluid pressure. H, C and M are stiffnesses that depend on the angular frequency ω. The model is viscoacoustic, which implies no shear deformations, i.e. μ is taken as 0. The stress–strain relationships (1)–(7) then simplify to

$$-p = \mathrm{He} - C\zeta \tag{8}$$

and

$$p_f = -Ce + M\zeta, \tag{9}$$

where p is the bulk hydrostatic stress. The assumption that the rigidity modulus vanishes is not restrictive for compressional waves. It is equivalent to considering a purely dilatational source, since in this case, the compressional and shear waves do not interact with each other if the medium is isotropic and homogeneous. It is convenient to express (8) and (9) in matrix forms as

$$\begin{bmatrix} p \\ p_f \end{bmatrix} = \begin{bmatrix} -H & C \\ -C & M \end{bmatrix} \begin{bmatrix} e \\ \zeta \end{bmatrix} \tag{10}$$

or, in compact notation,

$$\mathbf{P} = \mathbf{M} \cdot \mathbf{E}, \tag{11}$$

where $\mathbf{M}$ is the complex bulk modulus and the dot denotes the ordinary matrix product.

The explicit expression of this matrix is given in the next section. The high-frequency limit gives the elastic dynamic behaviour (e.g. Herrera and Gurtin 1965), implying that $\mathbf{M}(\infty)$ is the poroelastic (Biot) bulk modulus which, as shown by Carcione (1993), is given by

$$\mathbf{M}(\infty) = \begin{bmatrix} -H_\infty & C_\infty \\ -C_\infty & M_\infty \end{bmatrix}, \tag{12}$$

where

$$KH_\infty = \frac{1}{K_m} - \frac{1}{K_s} - \phi\left(\frac{1}{K_s} - \frac{1}{K_f}\right), \tag{13}$$

$$KC_\infty = \frac{1}{K_m} - \frac{1}{K_s} \tag{14}$$

and

$$KM_\infty = \frac{1}{K_m}, \tag{15}$$

with

$$K = \frac{\phi}{K_m}\left(\frac{1}{K_f} - \frac{1}{K_s}\right) + \frac{1}{K_s}\left(\frac{1}{K_m} - \frac{1}{K_s}\right), \tag{16}$$

where K_s, K_m and K_f are the bulk moduli of the solid, matrix and fluid, respectively, and ϕ is the effective porosity.

The dynamic equations were obtained by Biot using a macroscopic approach. Restricted to the viscoacoustic case, the equations (Biot 1962b) become

$$-\nabla(p - s) = \rho\ddot{\mathbf{u}} + \rho_f\ddot{\mathbf{w}} \tag{17}$$

and

$$-\nabla(p_f - s_f) = \rho_f\ddot{\mathbf{u}} + Y(q)\dot{\mathbf{w}}, \tag{18}$$

where $\mathbf{u}$ is the average displacement of the solid and $\mathbf{w}$ is the average displacement giving the flow of the fluid relative to the solid. A dot above the variable denotes time derivative.

The quantities s and s_f are the body forces acting on the matrix–fluid system and on the fluid phase, respectively. The composite density of the saturated material is $\rho = (1 - \phi)\rho_s + \phi\rho_f$, where ρ_s and ρ_f are the solid and fluid densities, respectively. The operator $Y(q)$ is a function of $q = d/dt$ which, for harmonic fields at the angular frequency ω, is $q = i\omega$. This is Biot's viscodynamic operator and describes the relative motion of the fluid. It depends on the fluid interia, its viscosity and the pore geometry. In the low-frequency range (Biot 1962b),

$$Y(q) = mq + \frac{\eta}{\kappa}, \qquad \text{for } \omega < \omega_c = \frac{\eta}{mk}, \tag{19}$$

where $m = \alpha\rho_f/\phi$, α is the tortuosity, a dimensionless parameter that is dependent on the pore geometry, η is the fluid viscosity and κ is the global permeability of the porous medium. The frequency ω_c defines the upper limit for which the fluid motion is dominated by Poiseuille viscous flow. In the high-frequency range,

$$Y(\omega) = \frac{\omega\rho_f}{i\phi}\frac{J_0(\sqrt{-6i\omega/\omega_c})}{J_2(\sqrt{-6i\omega/\omega_c})} \tag{20}$$

for a porous network represented by circular tubes (Auriault *et al.* 1985), where J_0 and J_2 are Bessel functions of the first kind, and the characteristic frequency is $\omega_c = 6\eta/a^2\rho_f$, where a is the radius of the tube (see Appendix). For $\omega \ll \omega_c$, $J_0/J_2 \approx -(4\omega_c/3i\omega)(1 + i\omega/\omega_c)$. In the limit, and using $\alpha = 4/3$, $Y(\omega)$ takes the form given in (19). Biot (1956c) introduced a *structural factor* δ that takes into account the sinuosity and cross-sectional shapes of the ducts. In this case, the argument of the Bessel functions in (20) is replaced by $\delta\sqrt{-i\omega/\omega_c}$. The viscodynamic operator for slit-like pores is given in the Appendix. Another strategy is to consider η and κ as empirical parameters and no explicit pore geometry. In practice, the viscodynamic term in (18) involves a convolution between $Y(t)$ and the corresponding fluid particle velocity $\dot{\mathbf{w}}$. As an illustration, in the Appendix we show the relationship between the Biot (1962a) and Auriault *et al.* (1985) formulations of the poroelastic equations.

In the harmonic regime, equations (17) and (18) can be written alternatively as

$$\nabla(\mathbf{P} - \mathbf{S}) = -\omega^2 \boldsymbol{\Gamma} \cdot \begin{bmatrix} \mathbf{u} \\ -\mathbf{w} \end{bmatrix}, \tag{21}$$

where

$$\mathbf{S} = [s, s_f]^T \tag{22}$$

and

$$\boldsymbol{\Gamma} \equiv \begin{bmatrix} -\rho & \rho_f \\ -\rho_f & Y/i\omega \end{bmatrix} \tag{23}$$

is the viscodynamic matrix.

The solution

Taking the divergence in (21) and assuming a homogeneous porous medium yields

$$\Delta(\mathbf{P} - \mathbf{S}) = -\omega^2 \boldsymbol{\Gamma} \cdot \mathbf{E}, \tag{24}$$

where

$$\mathbf{E} = \operatorname{div} \begin{bmatrix} \mathbf{u} \\ -\mathbf{w} \end{bmatrix}, \tag{25}$$

and Δ is the Laplacian operator. Substituting the constitutive law (11), (24) becomes

$$\Delta(\mathbf{P} - \mathbf{S}) + \omega^2 \mathbf{D} \cdot \mathbf{P} = 0, \tag{26}$$

where

$$\mathbf{D} = \boldsymbol{\Gamma} \cdot \mathbf{M}^{-1}. \tag{27}$$

Note that $\mathbf{D}$ is a complex function of the frequency and does not depend on the position vector since the medium is homogeneous. This matrix may be decomposed as $\mathbf{D} = \mathbf{A} \cdot \mathbf{\Lambda} \cdot \mathbf{A}^{-1}$, where $\mathbf{\Lambda}$ is the diagonal matrix of the eigenvalues, and $\mathbf{A}$ is a matrix whose columns are the right eigenvectors. Thus, substituting this decomposition into (26) and multiplying by $\mathbf{A}^{-1}$ from the right-hand side, yields

$$\Delta(\mathbf{V} - \mathbf{F}) + \omega^2 \mathbf{\Lambda} \cdot \mathbf{V} = 0, \tag{28}$$

where

$$\mathbf{V} = [v_1, v_2]^{\mathrm{T}} = \mathbf{A}^{-1} \cdot \mathbf{P}, \tag{29}$$

and

$$\mathbf{F} = [f_1, f_2]^{\mathrm{T}} = \mathbf{A}^{-1} \cdot \mathbf{S}. \tag{30}$$

From (28) we get the following Helmholtz equations for the components of $\mathbf{v}$:

$$(\Delta + \omega^2 \lambda_\nu) v_\nu = \Delta f_\nu, \qquad \nu = 1, 2, \tag{31}$$

where λ_1 and λ_2 are the eigenvalues of $\mathbf{D}$. It can be shown that they are related to the complex velocities of the fast and slow compressional waves. In fact, let us assume that a solution to (26) is of the form

$$\mathbf{P} = \mathbf{P}_0 \exp(\mathrm{i}\mathbf{k} \cdot \mathbf{x}), \tag{32}$$

where $\mathbf{x}$ is the position vector and $\mathbf{k}$ is the complex wavevector. Putting this solution into (26) with zero body forces, and setting the determinant to zero, gives the dispersion equation

$$\det\left[\mathbf{D} - \left(\frac{k}{\omega}\right)^2 \mathbf{I}\right] = 0, \tag{33}$$

where $\mathbf{I}$ is the identity matrix. Since $\omega/k \equiv V$ is the complex velocity, the eigenvalues of $\mathbf{D}$ are given by $\lambda = 1/V^2$. Since $\mathbf{D}$ is a second rank matrix, two modes propagate in the medium and correspond to the fast and slow waves. A simplified expression for the eigenvalues is

$$\lambda_{1(2)} = \frac{1}{2 \det \mathbf{M}} [U \pm \sqrt{U^2 - 4 \det \mathbf{M} \det \mathbf{\Gamma}}], \tag{34}$$

where

$$U = 2\rho_{\mathrm{f}} C - \rho M - H(Y/\mathrm{i}\omega). \tag{35}$$

Considering the solution for the Green's function (i.e. the right-hand side of (31) is a space delta function at, say, the origin), both equations have the form

$$(\Delta + \omega^2 \lambda) g = -8\delta(\mathbf{x}), \tag{36}$$

where δ is Dirac's distribution. The 2D solution (line source) of (36) is (Pilant 1979, p. 55)

$$g(r, \omega) = -2\mathrm{i}\mathrm{H}_0^{(2)}[\omega r\sqrt{\lambda(\omega)}], \tag{37}$$

where $\mathrm{H}_0^{(2)}$ is the Hankel function of the second kind, and

$$r = \sqrt{x^2 + z^2}. \tag{38}$$

The 3D solution (point source) of (36) is (Pilant 1979, p. 64)

$$g(r, \omega) = \frac{1}{r}\exp\left[-\mathrm{i}\omega r\sqrt{\lambda(\omega)}\right], \tag{39}$$

where

$$r = \sqrt{x^2 + y^2 + z^2}. \tag{40}$$

The solutions (50) and (52) as given by Pilant (1979) hold only for real arguments of the Hankel function. However, by invoking the correspondence principle (e.g. Ben-Menahem and Singh 1981), complex, frequency-dependent material properties can be considered. For instance, the poroelastic equations without the Biot mechanism (i.e. $\eta = 0$) have a real **D** matrix, whose eigenvalues are also real (velocities are real and constant, without frequency dispersion). The introduction of the Biot mechanism, by using the correspondence principle, implies the substitution $m \rightarrow -Y(\omega)/\mathrm{i}\omega$. In the same way, viscoelastic phenomena of a more general nature can be modelled.

The solution of (31), with the band-limited sources f_1 and f_2, is

$$v_\nu = \hat{f}_\nu \Delta g(\lambda_\nu) = \hat{f}_\nu G(\lambda_\nu), \tag{41}$$

where

$$G(\lambda_\nu) = -[\omega^2 \lambda_\nu g(\lambda_\nu) + 8\delta(\mathbf{x})], \tag{42}$$

and (36) has been used. In (41) we introduced the source vector

$$\hat{\mathbf{F}} = [\hat{f}_1, \hat{f}_2]^{\mathrm{T}} = \mathbf{A}^{-1} \cdot \hat{\mathbf{S}} h(\omega), \tag{43}$$

where

$$\hat{\mathbf{S}} = [\hat{s}, \hat{s}_{\mathrm{f}}]^{\mathrm{T}} \tag{44}$$

is a constant vector and $h(\omega)$ is the source frequency spectrum.

The vector **P** is obtained from (29),

$$\mathbf{P}(r, \omega) = \mathbf{A}(\omega)\mathbf{V}(r, \omega). \tag{45}$$

From the form of v_1 and v_2 in (41) and using (43), the solution can be explicitly written as

$$\mathbf{P} = \mathbf{A}\begin{bmatrix} G(\lambda_1) & 0 \\ 0 & G(\lambda_2) \end{bmatrix}\mathbf{A}^{-1}\hat{\mathbf{S}} h. \tag{46}$$

Using $\mathbf{D} = \mathbf{A} \cdot \mathbf{\Lambda} \cdot \mathbf{A}^{-1}$, and from the theory of functions of matrices (e.g. Lancaster and Tismenetsky 1985, p. 311), (46) becomes

$$\mathbf{P} = G(\mathbf{D}) \cdot \hat{\mathbf{S}}h, \tag{47}$$

where $G(\mathbf{D})$ can be viewed as the evolution operator (or Green's function) of the system. An effective numerical implementation of the evolution operator is obtained by decomposing it into its Lagrange interpolator (Lancaster and Tismenetsky 1985, p. 308). This yields

$$G(\mathbf{D}) = \frac{1}{\lambda_1 - \lambda_2} \{[G(\lambda_1) - G(\lambda_2)]\mathbf{D} + [\lambda_1 G(\lambda_2) - \lambda_2 G(\lambda_1)]\mathbf{I}\}. \tag{48}$$

This expression avoids the calculations of the eigenvectors of $\mathbf{D}$ (i.e. of matrix $\mathbf{A}$). Using (42) and the complex velocities $V_\nu = 1/\sqrt{\lambda_\nu}$, $\nu = 1, 2$, (48) becomes

$$G(\mathbf{D}) = \frac{\omega^2}{V_2^2 - V_1^2} \{[V_1^2 g(V_2) - V_2^2 g(V_1)]\mathbf{D} + [g(V_1) - g(V_2)]\mathbf{I}\} - 8\delta(\mathbf{x})\mathbf{I}. \tag{49}$$

In the absence of viscoelastic dissipation and with the Biot mechanism de-activated (i.e. zero fluid viscosity), only the Green's functions (37) and (39) are frequency dependent (the eigenvalues of $\mathbf{D}$ are real). Let us denote the phase velocities of the fast and slow waves as V_F and V_s, respectively. Then, the explicit frequency dependence of the evolution operator is

$$G(\mathbf{D}, \omega) = \frac{G(V_F, \omega)}{(V_S/V_F)^2 - 1} (V_S^2 \mathbf{D} - \mathbf{I}) - \frac{G(V_S, \omega)}{1 - (V_F/V_S)^2} (V_F^2 \mathbf{D} - \mathbf{I}). \tag{50}$$

In this case, the solution can be obtained in closed form since the Green's functions (37) and (39) can be Fourier transformed analytically to the time-domain (e.g. Norris 1985).

In order to ensure a time-domain real solution in the general viscoelastic case, we take

$$\mathbf{P}(r, \omega) = \mathbf{P}^*(r, -\omega), \tag{51}$$

for $\omega < 0$, where the superscript * denotes complex conjugate. Finally, the time-domain solution is obtained by an inverse Fourier transform.

Complex bulk moduli matrix, *Q* factors and phase velocities

There are two strategies to introduce general viscoelasticity in the theory. In the first approach, the solid, matrix and fluid bulk moduli in (13)–(15) are replaced by complex moduli, i.e.

$$K_u \rightarrow \bar{K}_u, \qquad \text{u denotes s, m or f.} \tag{52}$$

This defines the complex bulk moduli matrix $\mathbf{M}$ (see (10)). General frequency behaviour is modelled by several standard linear elements in parallel connection.

Such a model gives

$$\bar{K}_{\mathrm{u}} = \frac{K_{\mathrm{u}}}{L_{\mathrm{u}}} \sum_{l=1}^{L_{\mathrm{u}}} \frac{\tau_{\sigma l}^{(\mathrm{u})}}{\tau_{\varepsilon l}^{(\mathrm{u})}} \left[\frac{1 + \mathrm{i}\omega\tau_{\varepsilon l}^{(\mathrm{u})}}{1 + \mathrm{i}\omega\tau_{\sigma l}^{(\mathrm{u})}} \right], \tag{53}$$

where $\tau_{\sigma l}^{(\mathrm{u})}$ and $\tau_{\varepsilon l}^{(\mathrm{u})}$ are material relaxation times and L_{u} is the number of dissipation mechanisms. Note that when $\omega \to \infty$, $\bar{K}_{\mathrm{u}} \to K_{\mathrm{u}}$. Another useful kernel, to obtain a constant quality factor over a given frequency band, is constructed with a continuous distribution of relaxation mechanisms (Liu, Anderson and Kanamori 1976; Carcione 1993).

The quality factors of the solid, dry matrix and the fluid (which parameterized the model), are then given by

$$Q_{\mathrm{u}} = \frac{\mathrm{Re}\,[\bar{K}_{\mathrm{u}}]}{\mathrm{Im}\,[\bar{K}_{\mathrm{u}}]}, \qquad \mathrm{u\ denotes\ s,\ m,\ or\ f,} \tag{54}$$

For instance, when $L_{\mathrm{u}} = 1$,

$$Q_{\mathrm{u}} = Q_0^{(\mathrm{u})} \left(\frac{1 + \omega^2\tau_0^2}{2\omega\tau_0} \right), \tag{55}$$

where $Q_0^{(\mathrm{u})} = 2\tau_0/(\tau_{\varepsilon l}^{(\mathrm{u})} - \tau_{\sigma l}^{(\mathrm{u})})$ and $\tau_0 = \sqrt{\tau_{\varepsilon l}^{(\mathrm{u})}\tau_{\sigma l}^{(\mathrm{u})}}$. The curve $Q_{\mathrm{u}}(\omega)$ has its peak at $\omega_0 = 1/\tau_0$, and the value of Q_{u} at the peak is $Q_0^{(\mathrm{u})}$. The examples presented in the next section assume that ω_0 coincides with the central frequency of the source.

The second approach, used when modelling more complex phenomena than intrinsic dissipation of the single constituents, considers that the quantities H, C and M in (10) have a specific frequency dependence according to the anelastic process causing the dissipation.

The anelastic properties of the compressional waves are obtained from the characteristic equation (33). Having $\mathbf{M}$ and the viscodynamic matrix $\boldsymbol{\Gamma}$, we compute $\mathbf{D}$ from (27), diagonalize it and compute the complex velocities as

$$V_v = \frac{1}{\sqrt{\lambda_v}}, \qquad v = 1, 2, \tag{56}$$

where λ_1 and λ_2 are the eigenvalues of matrix $\mathbf{D}$, corresponding to the fast and slow waves, respectively, given in (34). For homogeneous viscoelastic waves, the phase velocities are given by the frequency divided by the real part of the complex wavenumber,

$$c_v = \left(\mathrm{Re} \left[\frac{1}{V_v} \right] \right)^{-1}. \tag{57}$$

The attenuation is the imaginary part of the complex wavenumber. In terms of the complex velocity,

$$\alpha_v = -\omega\ \mathrm{Im} \left[\frac{1}{V_v} \right]. \tag{58}$$

The quality factors can be expressed as

$$Q_u = \frac{\text{Re}\,[V_v^2]}{\text{Im}\,[V_v^2]}. \tag{59}$$

Equation (57) is an extension to porous media of the quality factors for homogeneous plane waves in a viscoelastic solid (Carcione, Kosloff and Kosloff 1988). A more precise expression for viscoelastic porous media is given by Rasolofosaon (1991).

Examples and discussion

The material properties of a porous brine-saturated sandstone medium are given in Table 1. Figures 1a and b represent the phase velocities of the compressional modes versus the frequency, corresponding to an acoustic skeleton saturated with water and oil, respectively. The slow wave has a diffusive character at low frequencies. When the saturating fluid is oil ($\eta = 264$ cp), the diffusive behaviour invades higher frequencies. Figure 1c shows the attenuation α_2 of the slow wave versus the frequency; the higher the frequency, the higher the dissipation. This phenomenon and the diffusive character of the slow wave at low frequencies make it difficult to detect this wave experimentally over the whole frequency range.

In the following, we analyse the 3D pressure wavefields by varying some of the material parameters in Table 1: the frequency range, the dimensionality of the space, the type of source (see Appendix) and the intrinsic solid and fluid dissipations. Instead of the bulk hydrostatic stress p, we plot the pressure in the solid phase, which is given by (Biot 1962a)

$$p_s = p - \phi p_f. \tag{60}$$

Table 1. Material properties: Brine saturated sandstone. 1 cp = 10^{-3} Pa s; 1 mD = 10^{-15} m^2.

Solid	bulk modulus K_s	40 GPa
	density ρ_s	2500 kg/m^3
Matrix	bulk modulus K_m	20 GPa
	density ρ_m	2000 kg/m^3
	porosity ϕ	0.2
	permeability κ	600 mD
	tortuosity α	2
Fluid	bulk modulus K_f	2.5 GPa
	density ρ_f	1040 kg/m^3
	viscosity η	1 cp

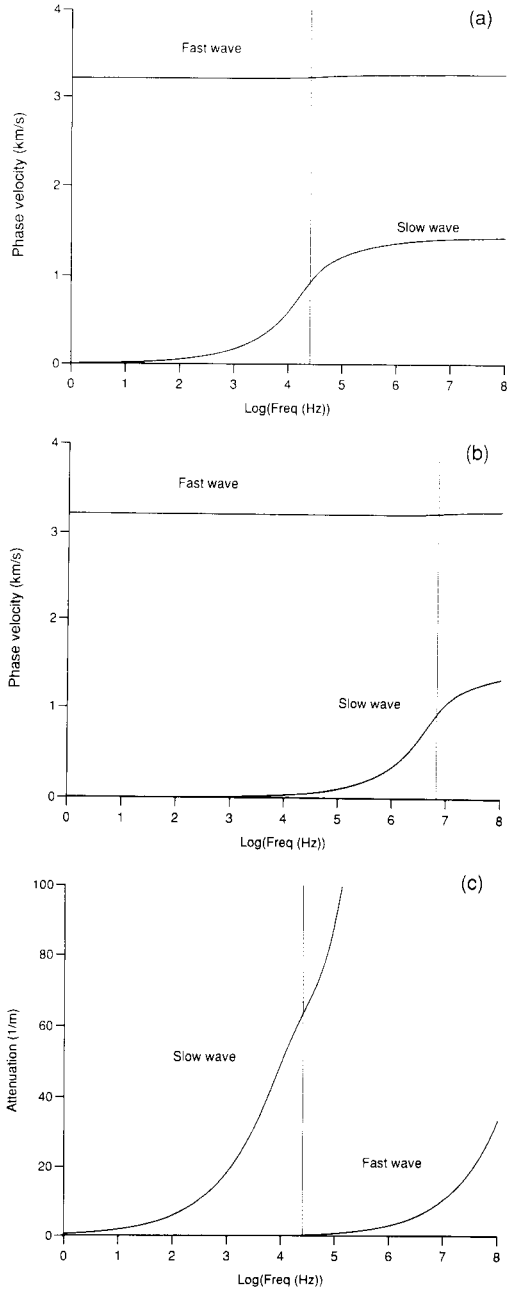

Figure 1. Phase velocity of the fast and slow compressional waves versus frequency of (a) the brine-saturated and (b) the soil-saturated sandstone. (c) shows the attenuation of the compressional waves versus frequency for the brine-saturated sandstone. The vertical line indicates the characteristic frequency.

In all cases, we model the full frequency range response by using the viscodynamic operator given in (20). The source time function is

$$h(t) = \exp\left[-\tfrac{1}{2}f_c^2(t-t_0)^2\right]\cos\left[\pi f_c(t-t_0)\right], \tag{61}$$

where f_c is the central frequency and $t_0 = 3/f_c$. The response of the medium is obtained by multiplying the Green's function (49) by the time Fourier transform of the wavelet, and then performing an inverse discrete Fourier transform back to the time domain. The time scale varies from seconds to microseconds in order to study the behaviour of the wavefield at different frequencies. The examples cover the seismic exploration band and frequency ranges used in laboratory experiments.

Viscosity

Consider a solid source with a central frequency of $f_c = 5$ MHz. The viscosity varies from that of brine, $\eta = 1$ cp, to that of oil, $\eta = 264$ cp (Fig. 2). The amplitudes of the fast wave in the solid and fluid phases remain unchanged. However, the amplitude of the fluid dilatation, corresponding to the fast wave, approaches that of the solid when the saturating fluid is oil. In this case, viscosity effects dominate over inertial effects and the material behaves as a single medium. The pressures differ since the solid and fluid bulk moduli are different. For the same reason, the slow wave disappears when the viscosity increases. Note also that this wave contributes mainly to the fluid pressure.

Porosity

Here the viscosity is set at zero (ideal fluid), and the central frequency of the source is $f_c = 25$ Hz, i.e. in the seismic exploration band. The porosity varies from 20% to 1%. In this experiment, the bulk modulus of the matrix and the tortuosity change with the porosity. We consider that $K_m = K_s(1 - 1.2\phi)$ and $\alpha = 0.5(1 + 1/\phi)$. The last equation was proposed by Berryman (1980) and corresponds to the case of solid spherical particles in a fluid. Figure 3 illustrates the phase velocity as a function of the porosity. As can be seen, the velocities of fast and slow waves decrease and increase, respectively, with increasing porosity. This is in agreement with the experimental curves obtained by Plona (1982). The transient response for a bulk source is shown in Fig. 4. The arrival times of the waves for the different porosities agree with the results plotted in Fig. 3; for lower porosity, the waves tend to separate. Moreover, the solid pressure decreases compared to the slow-wave fluid pressure.

Permeability

For brine saturation and a frequency $f_c = 0.5$ MHz, the wave-field is computed for different permeabilities (Fig. 5). The porosity and the tortuosity are kept constant

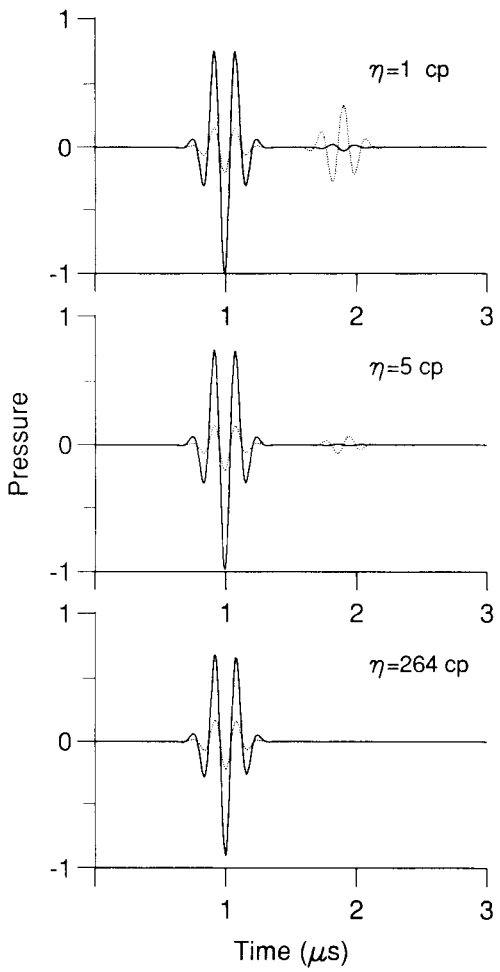

Figure 2. Transient response due to a solid source with a central frequency of $f_c = 5$ MHz, for different viscosities of the saturating fluid. The solid and dashed lines correspond to solid pressure p_s and fluid pressure p_f, respectively. Amplitudes are normalized with respect to the maximum value of the solid pressure, corresponding to $\eta = 1$ cp. The source–receiver distance is 2.25 mm.

for variable permeability. A more realistic analysis should consider, for instance, the Carman–Kozeny equation (Carman 1961). The variation of the permeability mainly affects the slow wave. As expected (see (19)), the effect is the inverse of that of the viscosity, i.e. lower permeability implies stronger dissipation of the slow wave.

Dimensionality of the space

Figure 6 shows the 2D and the 3D wavefields. The latter preserves the shape of the Ricker wavelet, since this is basically convolved with a Green's function containing

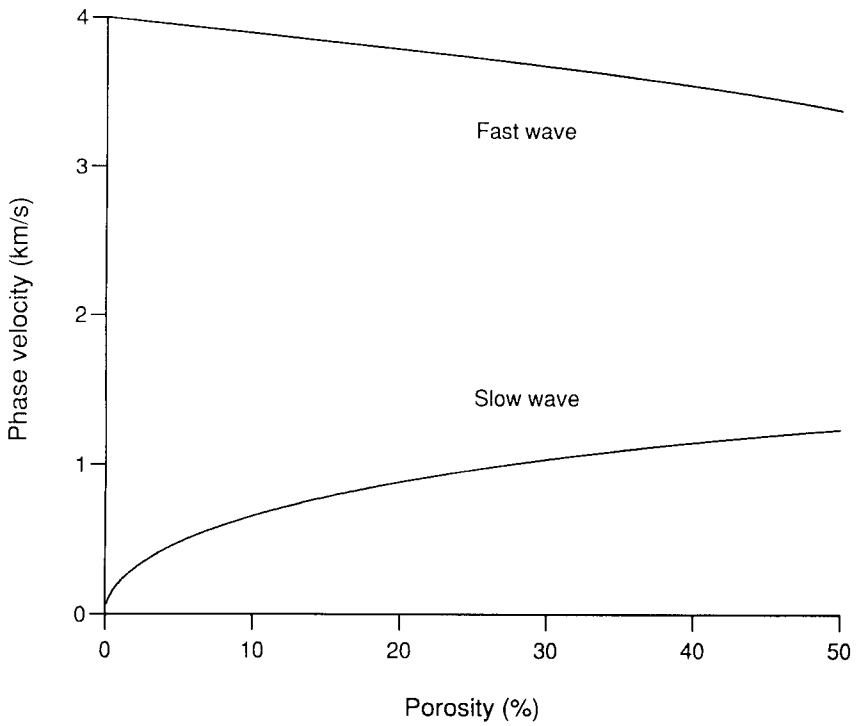

Figure 3. Phase velocities of the compressional waves versus porosity when viscosity effects are ignored.

delta functions (i.e. the inverse Fourier transform of (39), in the absence of viscoelasticity). The 2D response involves the transform of the Hankel's function, producing a change of shape.

Source type

Consider three source configurations (Fig. 7), whose analytical implementations in the equation of motion are analysed in the Appendix. In the absence of viscosity effects, the slow wave in the fluid has the higher amplitude, even when the source is in the solid. The slow wave in the fluid is out of phase with respect to the slow wave in the solid, in agreement with the differential motion that generates this phenomenon. On the other hand, the fast wave pressures are in phase. Moreover, the polarity of the slow wave for a solid source is opposite to that of the fluid and bulk sources. There is a critical value of the partition coefficient (fluid and solid contributions) of the source function for which no slow wave is generated (see Fig. 8). As indicated in the Appendix, a bulk source has $s_f = s$. The example shown in Figure 8 has $s_f = 0.225$ s, implying a solid–fluid coefficient equal to $(1/(0.225/\phi) - 1)$.

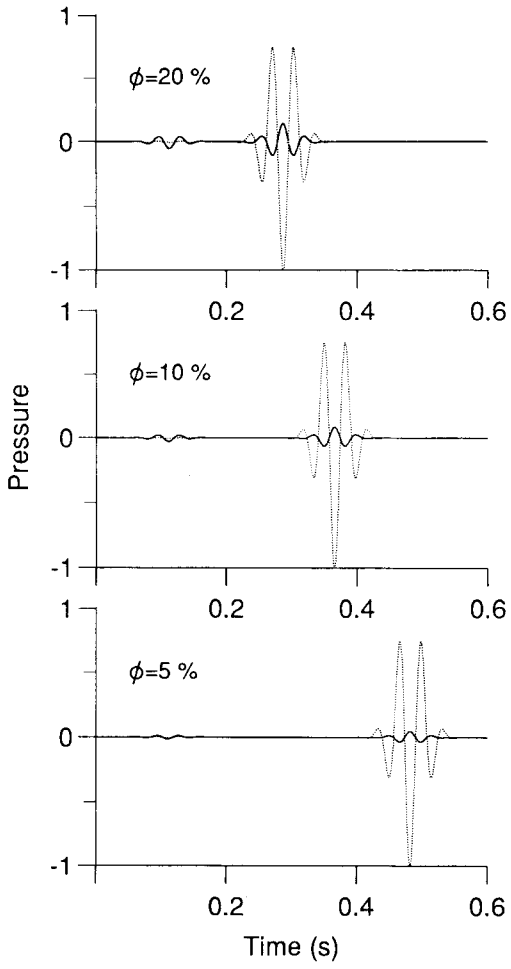

Figure 4. Transient response for three different porosities of a sandstone saturated with an ideal fluid ($\eta = 0$). The source is in the bulk material and has a central frequency of 25 Hz. The solid and dashed lines correspond to solid pressure p_s and fluid pressure p_f, respectively. Amplitudes are normalized with respect to the maximum value of the fluid pressure. The source–receiver distance is 200 m.

Intrinsic dissipation

The effects of matrix, solid and fluid dissipation are shown in Figs 9, 10 and 11, respectively. The fluid is ideal and the source is applied to the bulk material with a central frequency of 25 Hz. The quality factors $Q_0^{(u)}$, u denotes m, s or f, take the values ∞ (elastic case), 50 and 10. When solid dissipation is considered, the quality factor of the matrix is half the quality factor of the solid phase. Figure 9 corresponds to a viscoelastic skeleton, i.e. K_m is replaced by a complex modulus $\bar{K}_m$ as

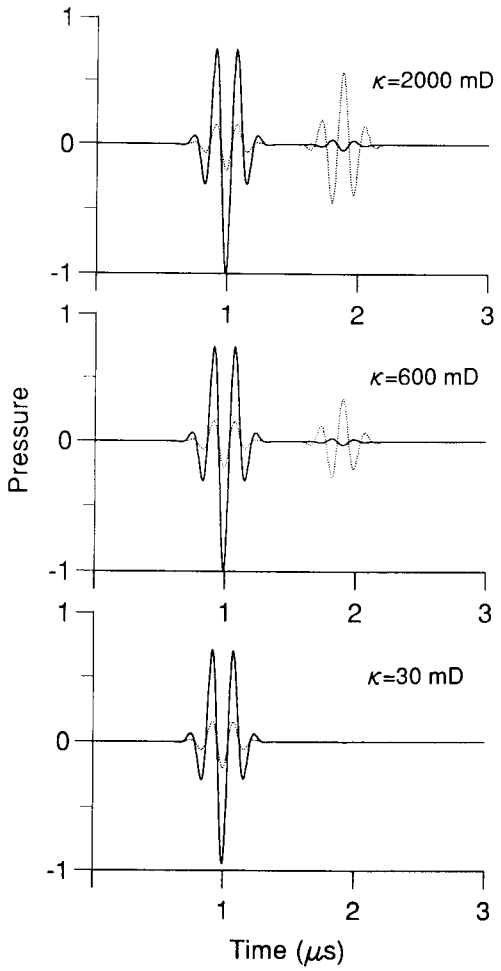

Figure 5. Transient response for three different permeabilities of a brine-saturated sandstone. The source is in the solid phase and has a central frequency of 0.5 MHz. The solid and dashed lines correspond to solid pressure p_s and fluid pressure p_f, respectively. Amplitudes are normalized with respect to the maximum value of the solid pressure, corresponding to $\kappa = 2000$ mD. The source–receiver distance is 2.25 mm.

given by (53). According to Biot (1962a), this simulates the squirt-flow dissipation mechanism by which a force applied to the area of contact between two grains produces a displacement of the surrounding fluid in and out of this area. Since the fluid is viscous, the motion is not instantaneous and energy dissipation occurs. The grains and the fluid are elastic and do not dissipate energy. The physics of the mechanism is contained in the operator describing the behaviour of the dry skeleton. Since experiments indicate that the mechanism can be represented by a Zener model (e.g. Murphy *et al.* 1986), we use one element in (53). Figure 9 indicates that

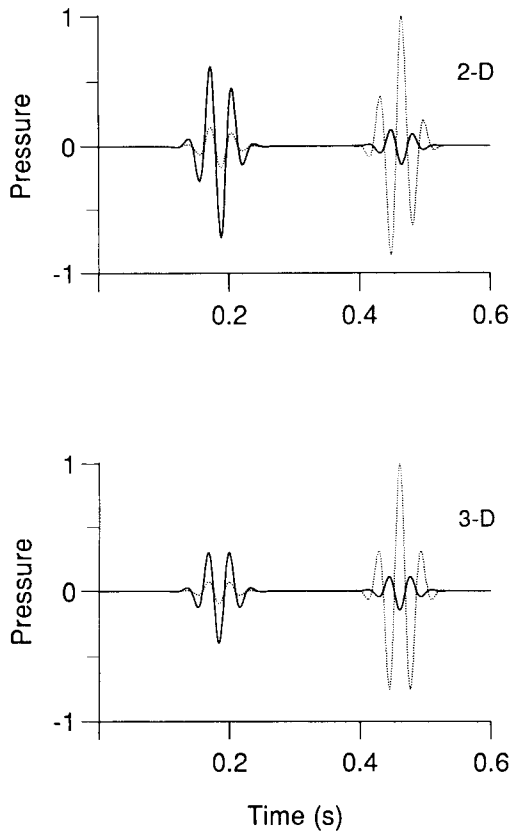

Figure 6. Transient response of a sandstone saturated with an ideal fluid comparing 2D and 3D wave propagation. The source is in the solid phase and has a central frequency of 25 Hz. The solid and dashed lines correspond to solid pressure p_s and fluid pressure p_f, respectively. Amplitudes are normalized with respect to the maximum value of the fluid pressure. The source–receiver distance is 400 m.

the squirt-flow mechanism affects both pressures, but mainly that of the slow wave, which shows a substantial energy dissipation for $Q_m = 10$. On the other hand, dissipation in the fluid does not have a major influence on the amplitude of the fast wave but strongly attenuates the slow pulse. In all the cases, the change in pulse shape is due to velocity dispersion.

Frequency range

Figure 12 shows the behaviour of the wavefield as a function of the frequency content of the (solid) source. Higher frequencies excite a slow wave that is stronger in the fluid phase. Increasing the frequency presents the same qualitative behaviour as decreasing the viscosity (compare Figs 2 and 12).

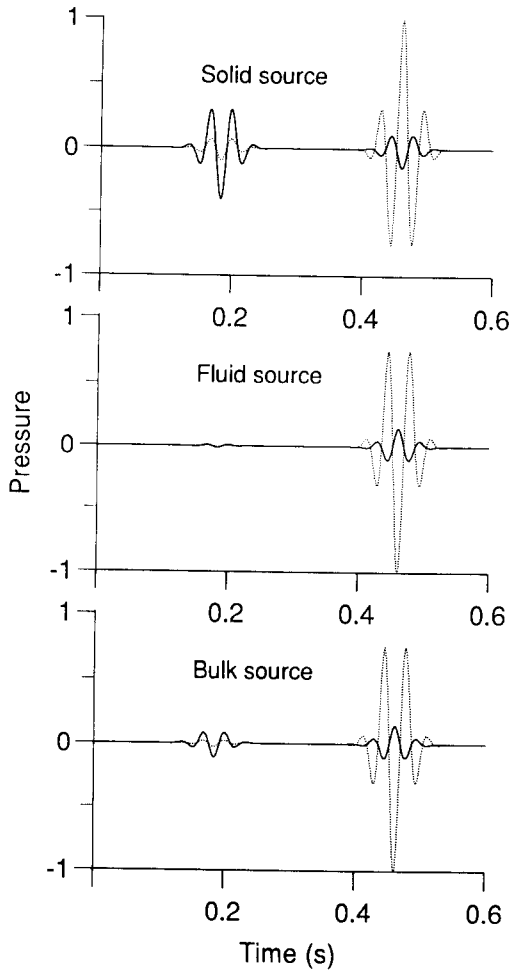

Figure 7. Transient response of a sandstone saturated with an ideal fluid ($\eta = 0$) for three different source excitations having a central frequency of 25 Hz. The solid and dashed lines correspond to solid pressure p_s and fluid pressure p_f, respectively. Amplitudes are normalized with respect to the maximum value of the fluid pressure. The source–receiver distance is 400 m.

Static mode

When the fluid is viscous, the slow wave becomes diffusive and appears as a static mode at the source location. This behaviour is predicted by the analytical solution (Fig. 13), where snapshots of the solid and fluid pressures due to a fluid volume injection are represented. The frequency band corresponds to the sonic range ($f_c = 4.5$ KHz) and the propagation time is 1.5 ms. In order to enhance the lower frequencies, we use the source spectrum $h(\omega)/i\omega$, which corresponds to the time

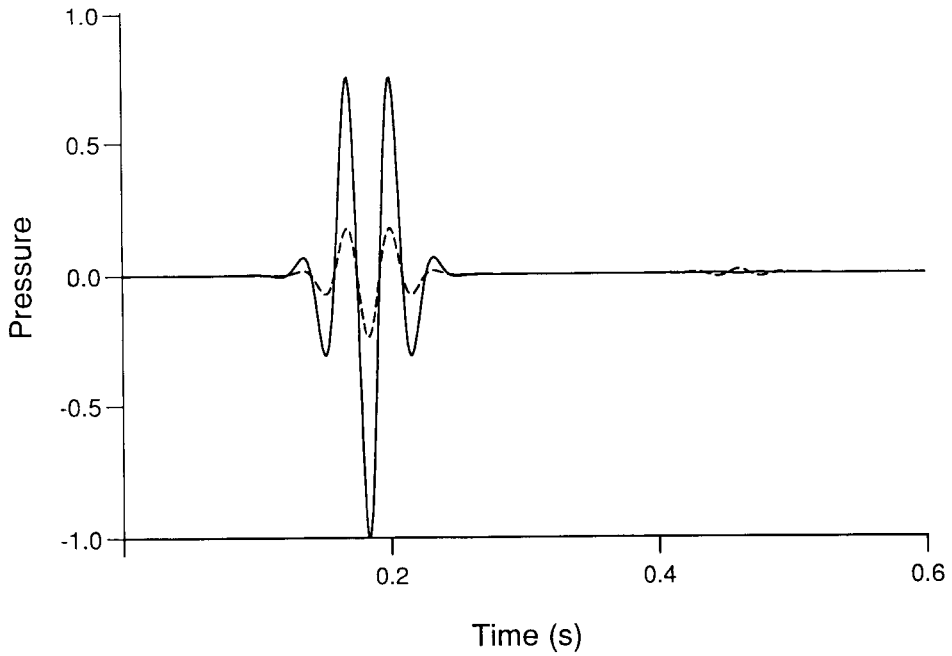

Figure 8. Transient response of a sandstone saturated with an ideal fluid ($\eta = 0$) for a solid–fluid source partition coefficient equal to 21. The solid and dashed lines correspond to solid pressure p_s and fluid pressure p_f, respectively. Amplitudes are normalized with respect to the maximum value of the solid pressure. The dominant frequency is 25 Hz and the source–receiver distance is 400 m.

integral of $h(t)$. This allows a better excitation of the static mode as can be inferred from its attenuation curve (Fig. 1c).

A more general soluton for wave propagation in a porous medium should consider partial saturation, i.e. the presence of a two-phase fluid. Recent work (Berryman, Thigpen and Chin 1988; Santos *et al.* 1990a, b) indicates that in this case there exist two slow waves with very low velocity compared to the compressional waves travelling in a saturated material.

Conclusions

Reservoir characterization from wave propagation experiments requires a mathematical model which accounts for the effects of rock and fluid stiffnesses, porosity, fluid viscosity and permeability on wave characteristics. Biot's theory allows an explicit treatment of these properties and is the framework for building a general model including complex mechanisms for wave dissipation and velocity dispersion. The first stage in understanding the physics of wave propagation is to study the

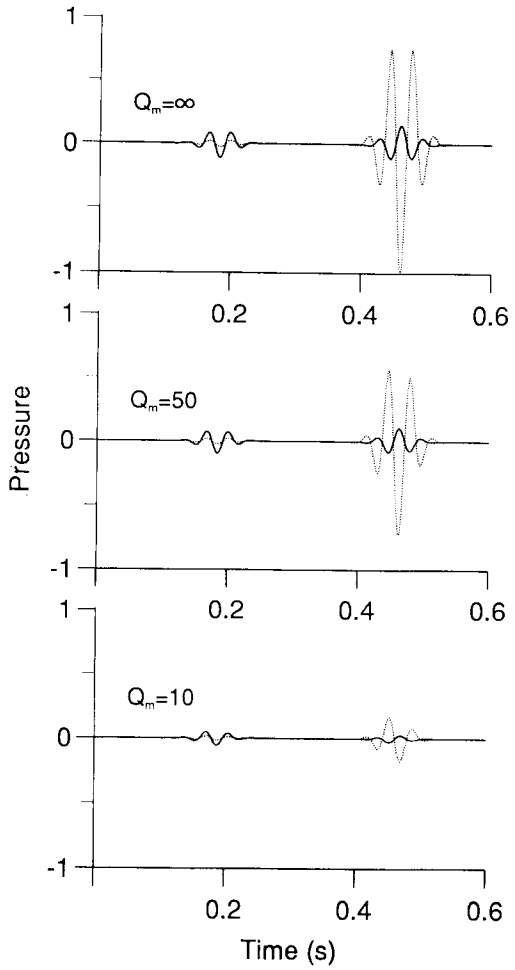

Figure 9. Transient response of a sandstone saturated with an ideal fluid ($\eta = 0$) for three different levels of attenuation of the skeleton (squirt-flow mechanism). The solid and dashed lines correspond to solid pressure p_s and fluid pressure p_f, respectively. Amplitudes are normalized with respect to the maximum value of the fluid pressure, corresponding to the elastic case. The source is in the bulk material at a distance of 400 m from the receiver and has a central frequency of 25 Hz.

influence of the material properties when the medium between the source and the receiver is homogeneous. For this purpose, an analytical solution for the propagation of compressional waves is presented. We use the concept of the viscodynamic operator to account for the dynamic properties of the fluid motion, and a phenomenological viscoelastic model introduces anelastic effects due the variety of complex dissipation mechanisms.

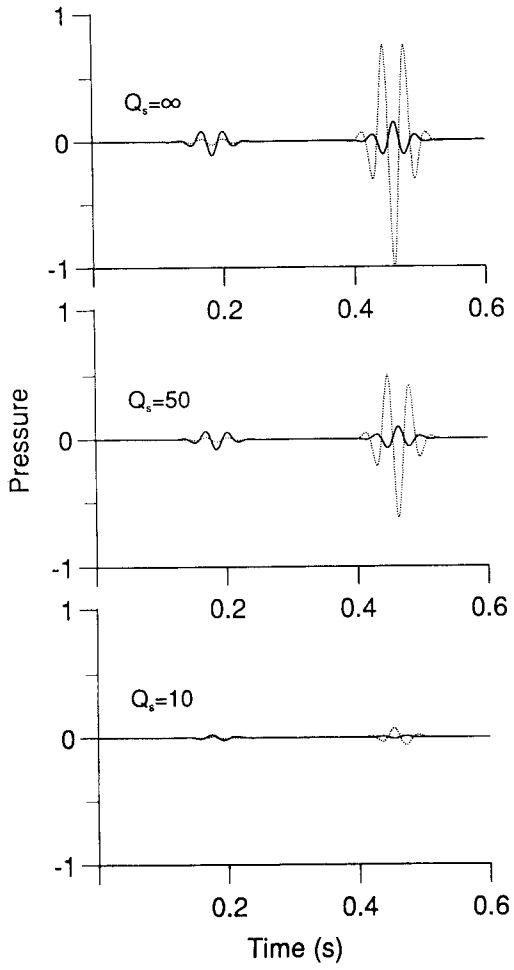

Figure 10. Transient response of a sandstone saturated with an ideal fluid ($\eta = 0$) for three different levels of attenuation of the solid phase. The solid and dashed lines correspond to solid pressure p_s and fluid pressure p_f, respectively. Amplitudes are normalized with respect to the maximum value of the fluid pressure, corresponding to the elastic case. The source is in the bulk material at a distance of 400 m from the receiver and has a central frequency of 25 Hz.

The most relevant results obtained from the analysis are:

1. The slow wave is stronger in the fluid phase.
2. The slow wave in the fluid is out of phase with respect to the slow wave in the solid.
3. When brine is replaced by oil, the slow wave disappears and the material behaves as a single medium.
4. The slow wave in the solid decreases in amplitude as porosity decreases.

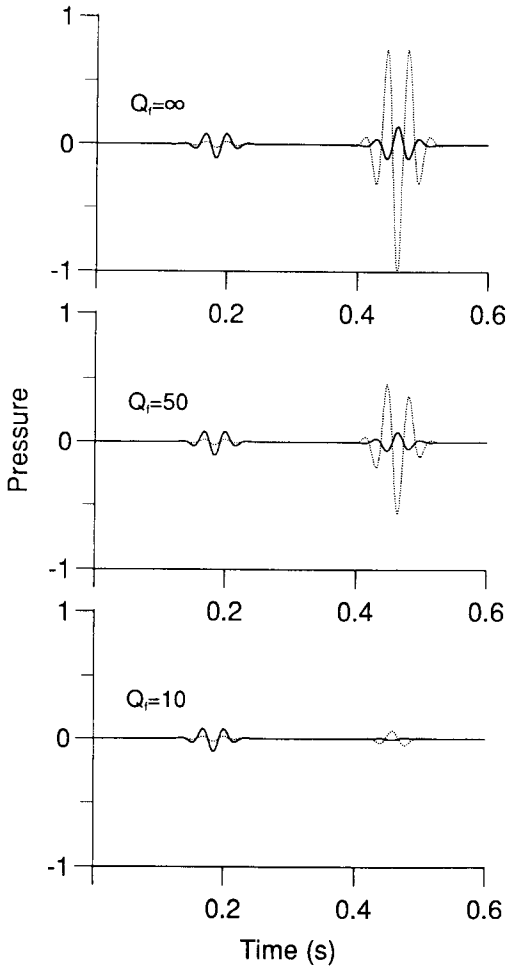

Figure 11. Transient response of a sandstone saturated with an ideal fluid ($\eta = 0$) for three different levels of attenuation of the fluid phase. The solid and dashed lines correspond to solid pressure p_s and fluid pressure p_f, respectively. Amplitudes are normalized with respect to the maximum value of the fluid pressure, corresponding to the elastic case. The source is in the bulk material at a distance of 400 m from the receiver and has a central frequency of 25 Hz.

5. A fluid injection source transfers most of its energy to slow-wave motion in the fluid phase.

6. There is a critical value of the partition coefficient (fluid and solid contributions) of the source for which no slow wave is generated.

7. For low permeability, the slow wave disappears and the material behaves as a single medium.

8. The squirt-flow mechanism and intrinsic solid dissipation attenuate both types of wave. The slow wave shows a substantial change of shape due to velocity disper-

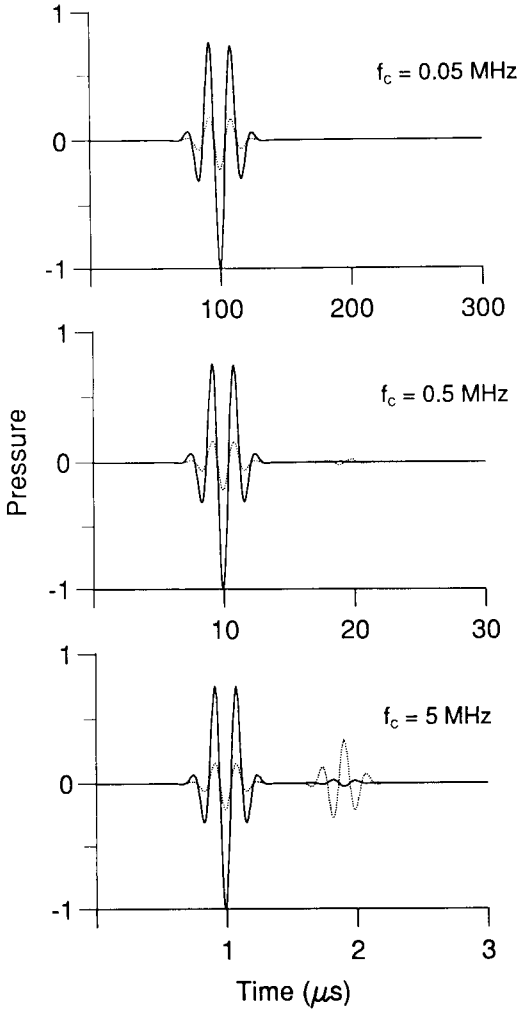

Figure 12. Transient response of a brine-saturated sandstone as a function of the frequency content of the (solid) source. The solid and dashed lines correspond to solid pressure p_s and fluid pressure p_f, respectively. Amplitudes are normalized with respect to the maximum value of the solid pressure. From the low to the high frequencies, the source–receiver distances are 2.25 m, 2.25 cm and 2.25 mm, respectively.

Figure 13. Snapshots of (a) the solid and (b) the fluid pressure at 1.5 ms propagation time for a viscous pore fluid ($\eta \neq 0$). The source is a fluid volume injection and has a central frequency of 4.5 KHz. The event at the source location is the slow static mode.

(a) Solid pressure

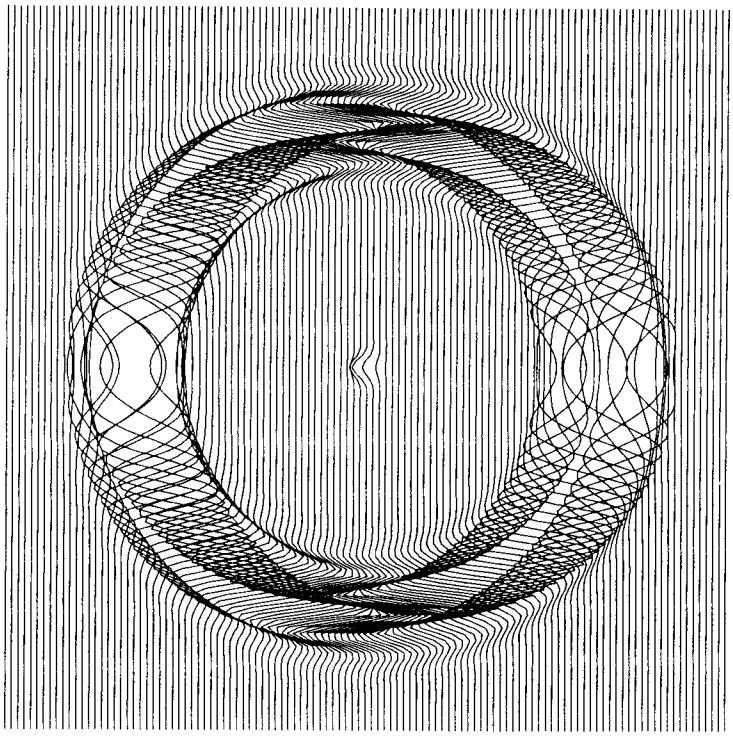

(b) Fluid pressure

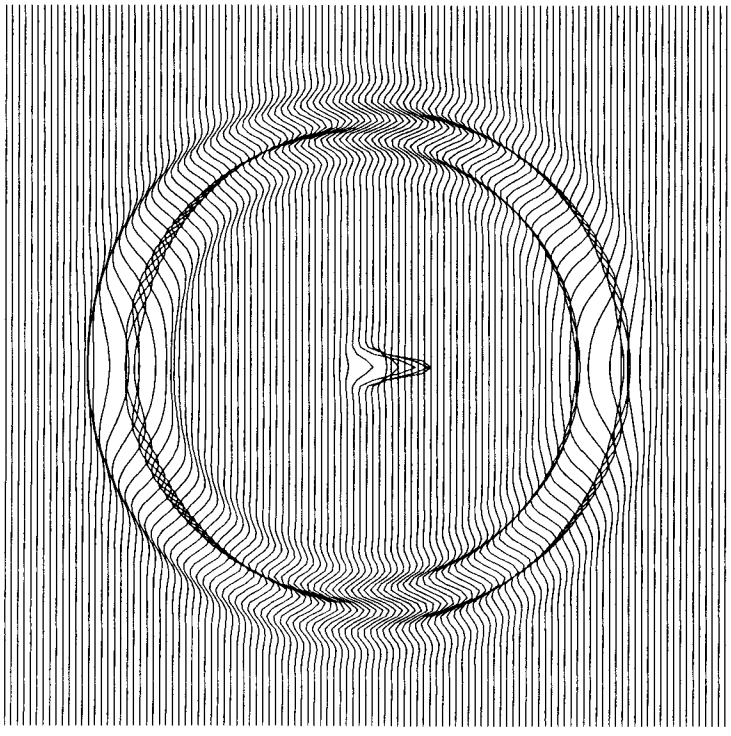

sion. On the other hand, dissipation in the fluid does not have a major influence on the amplitude of the fast wave.

9. When the pore fluid is viscous, the slow wave appears as a static mode at the source position.

Besides the analysis of the kinematic and dynamic characteristics of the wave motion, the present solution can be used to check the validity of numerical forward modelling algorithms.

Acknowledgements

This work was funded in part by the European Commission in the framework of the JOULE programme, sub-programme Advanced Fuel Technologies. Dr. Fabio Cavallini kindly read the manuscript and made helpful suggestions.

Appendix A

Relationship between the poroelastic equations of Biot and Auriault *et al.*

Auriault *et al.* (1985) use a homogenization theory to provide a unified expression for the mass and viscous coupling coefficients through a complex and frequency-dependent Darcy coefficient $K(\omega)$, which depends upon the shape and geometry of the pores. The equations are generally expressed in terms of the solid and fluid displacements $\mathbf{u}$ and $\mathbf{U}$, respectively, which corresponds to the formulation given by Biot (1956a). The acoustic equations (i.e. zero rigidity modulus) for time harmonic fields obtained by Auriault *et al.* (1985) (see also Boutin *et al.* 1987; Schmitt, Bouchon and Bonnet 1988) are

$$A\nabla \operatorname{div} \mathbf{u} + Q\nabla \operatorname{div} \mathbf{U} = \rho_{11}\ddot{\mathbf{u}} + \rho_{12}\ddot{\mathbf{U}} + b(\dot{\mathbf{u}} - \dot{\mathbf{U}}) + \mathbf{f}_s \tag{A1}$$

and

$$Q\nabla \operatorname{div} \mathbf{u} + R\nabla \operatorname{div} \mathbf{U} = \rho_{12}\ddot{\mathbf{u}} + \rho_{22}\ddot{\mathbf{U}} - b(\dot{\mathbf{u}} - \dot{\mathbf{U}}) + \mathbf{f}_f, \tag{A2}$$

where A, Q and R are the Biot elastic elastic coefficients (Biot and Willis 1957), and

$$b(\omega) = \phi^2 H_1(\omega), \tag{A3}$$

$$\rho_{22}(\omega) = \phi^2 H_2(\omega)/\omega, \tag{A4}$$

$$\rho_{12}(\omega) = \phi\rho_f - \rho_{22}(\omega) \tag{A5}$$

and

$$\rho_{11}(\omega) = (1 - \phi)\rho_s - \rho_{12}(\omega), \tag{A6}$$

with $H_1(\omega) + iH_2(\omega) = 1/K(\omega)$. For instance, a pore network of circular tubes of radius a has (Auriault *et al.* 1985)

$$K(\omega) = \frac{i\phi}{\omega\rho_f}\frac{J_2(s)}{J_0(s)}, \qquad \text{where } s = ia\left(\frac{i\omega\rho_f}{\eta}\right)^{1/2}, \tag{A7}$$

and for a pore network of plane slits of thickness $2a$,

$$K(\omega) = -\frac{i\phi}{\omega\rho_f}\left[1 - \frac{1}{s}\tan(s)\right]. \tag{A8}$$

Vectors $\mathbf{f}_s$ and $\mathbf{f}_s$ are external forces acting on the solid and fluid phases, respectively (Biot 1956b).

On the other hand, the elastic coefficients in equations (1)–(7) are related to the corresponding coefficients in (A1) and (A2) by (Biot 1962a)

$$H = A + R + 2Q, \qquad C = \frac{Q+R}{\phi}, \qquad M = \frac{R}{\phi^2}. \tag{A9}$$

In fact, in the absence of viscoelasticity we should consider H_∞, C_∞ and M_∞, as defined in (13)–(16), instead of H, C and M, which depend on frequency. Moreover, the following relationship hold (Biot 1962a)

$$\text{div } \mathbf{u} = e, \qquad \text{div } U = \varepsilon, \qquad -\text{div } \mathbf{w} = \zeta, \tag{A10}$$

and

$$\mathbf{w} = \phi(\mathbf{U} - \mathbf{u}), \qquad \zeta = \phi(e - \varepsilon). \tag{A11}$$

Using these relationships, (A1) and (A2) can be expressed as

$$A\nabla e + Q\nabla\left(e - \frac{\zeta}{\phi}\right) = \rho_{11}\ddot{\mathbf{u}} + \rho_{12}\left(\ddot{\mathbf{u}} + \frac{\ddot{\mathbf{w}}}{\phi}\right) - \frac{b}{\phi}\dot{\mathbf{w}} + \mathbf{f}_s \tag{A12}$$

and

$$Q\nabla e + R\nabla\left(e - \frac{\zeta}{\phi}\right) = \rho_{12}\ddot{\mathbf{u}} + \rho_{22}\left(\ddot{\mathbf{u}} + \frac{\ddot{\mathbf{w}}}{\phi}\right) + \frac{b}{\phi}\dot{\mathbf{w}} + \mathbf{f}_f. \tag{A13}$$

Adding these two equations we obtain

$$(A + 2Q + R)\nabla e - \left(\frac{Q+R}{\phi}\right)\nabla\zeta = (\rho_{11} + 2\rho_{12} + \rho_{22})\ddot{\mathbf{u}} + \left(\frac{\rho_{12} + \rho_{22}}{\phi}\right)\ddot{\mathbf{w}} + \mathbf{f}_s + \mathbf{f}_f \tag{A14}$$

Rearranging (A13) and dividing by ϕ, we obtain

$$\left(\frac{Q+R}{\phi}\right)\nabla e - \frac{R}{\phi^2}\nabla\zeta = \left(\frac{\rho_{12} + \rho_{22}}{\phi}\right)\ddot{\mathbf{u}} + \frac{\rho_{22}}{\phi^2}\ddot{\mathbf{w}} + \frac{b}{\phi^2}\dot{\mathbf{w}} + \frac{b}{\phi^2}\dot{\mathbf{w}} + \frac{\mathbf{f}_f}{\phi}. \tag{A15}$$

From (A3) and (A6), we have

$$\rho_{11}(\omega) + 2\rho_{12}(\omega) + \rho_{22}(\omega) = (1 - \phi)\rho_s + \phi\rho_f = \rho, \tag{A16}$$

the composite density, and

$$\frac{\rho_{12}(\omega) + \rho_{22}(\omega)}{\phi} = \rho_f. \tag{A17}$$

Moreover,

$$\frac{\rho_{22}(\omega)}{\phi^2} = \frac{H_2(\omega)}{\omega} = m(\omega), \tag{A18}$$

and

$$\frac{b(\omega)}{\phi^2} = H_1(\omega) = \frac{\eta}{\kappa}(\omega). \tag{A19}$$

The last two equations give

$$\frac{1}{K(\omega)} = H_1(\omega) + \mathrm{i}H_2(\omega) = \frac{\eta}{\kappa}(\omega) + \mathrm{i}\omega m(\omega) = Y(\omega), \tag{A20}$$

which is the viscodynamic operator introduced by Biot (1956c, 1962b). The explicit frequency dependence in η/κ and m means that they are defined for the whole frequency range. Finally, by using the preceding relationships, (A14) and (A15) become

$$H\nabla e - C\nabla\zeta = \rho\ddot{\mathbf{u}} + \rho_f\ddot{\mathbf{w}} + \mathbf{f}_s + \mathbf{f}_f \tag{A21}$$

and

$$C\nabla e + M\nabla\zeta = \rho_f\ddot{\mathbf{u}} + Y(\omega)\dot{\mathbf{w}} + \frac{\mathbf{f}_f}{\phi}, \tag{A22}$$

which are equivalent to (17) and (18), provided that $\nabla s = -(\mathbf{f}_s + \mathbf{f}_f)$ and $\nabla s_f = -\mathbf{f}_f/\phi$. Since we consider dilatational excitations, the relevant quantity is $\Delta\mathbf{S}$ (see (24)), and the number of independent scalar sources is two.

Consider three source types:

1. Bulk source: this situation, implemented, for instance, by Hassanzadeh (1991) and Dai *et al.* (1995), assumes that the source energy is partitioned linearly between the two phases as $\mathbf{f}_s = (1 - \phi)\mathbf{f}$ and $\mathbf{f}_f = \phi\mathbf{f}$. Then, we have that $\nabla s = \nabla s_f = \mathbf{f}$.
2. Source in the solid: We simply assume that $\mathbf{f}_f = 0$, implying that $\nabla s = \mathbf{f}_s$ and $\nabla s_f = 0$.
3. Fluid volume injection: In this case, $\mathbf{f}_s = 0$. Then, $\nabla s = \mathbf{f}_f$ and $\nabla s_f = \mathbf{f}_f/\phi$.

The transition from the low- to the high-frequency range of the theory is given by the characteristic frequency

$$\omega_c = a\frac{b(0)}{\rho_{22}(0)} = \frac{\eta}{m\kappa}, \tag{A23}$$

where a is the pore radius. Substituting the tortuosity $\alpha = m\phi/\rho_f$, we have

$$\omega_c = \frac{\eta\phi}{\alpha\kappa\rho_f}. \tag{A24}$$

For the model of cylindrical ducts $\alpha = 4/3$, $\kappa = \phi a^2/8$, and

$$\omega_c = \frac{6\eta}{a^2\rho_f}. \tag{A25}$$

Below ω_c (i.e. in the low-frequency range), viscous forces are predominant and the fluid is of the Poiseuille type. Moreover, ω_c determines the transition from a diffusive to a propagative slow compressional wave. Note that the argument of the Bessel functions in (A7) can be written in terms of the characteristic frequency as $s = (-6i\omega/\omega_c)^{1/2}$, which is the form given by Norris (1986, 1989) with the opposite sign convention for the Fourier transform.

References

Auriault J.L., Borne L. and Chambon R. 1985. Dynamics of porous saturated media, checking of the generalized law of Darcy. *Journal of the Acoustical Society of America* 77, 1641–1650.

Ben-Menahem A.B. and Singh S.J. 1981. *Seismic Waves and Sources*. Springer Verlag, Inc.

Berryman J.G. 1980. Confirmation of Biot's theory. *Applied Physics Letters* 37, 382–384.

Berryman J.G., Thigpen L. and Chin R.C.Y. 1988. Bulk elastic wave propagation in partially saturated porous solids. *Journal of the Acoustical Society of America* 84, 360–373.

Biot M.A. 1956a. Theory of deformation of a porous viscoelastic anisotropic solid. *Journal of Applied Physics* 27, 459–467.

Biot M.A. 1956b. Theory of propagation of elastic waves in a fluid-saturated porous solid. I. Low-frequency range. *Journal of the Acoustical Society of America* 28, 168–178.

Biot M.A. 1956c. Theory of propagation of elastic waves in a fluid-saturated porous solid. II. Higher frequency range. *Journal of the Acoustical Society of America* 28, 179–191.

Biot M.A. 1962a. Mechanics of deformation and acoustic propagation in porous media. *Journal of Applied Physics* 33, 1482–1498.

Biot M.A. 1962b. Generalized theory of acoustic propagation in porous dissipative media. *Journal of the Acoustical Society of America* 34, 1254–1264.

Biot M.A. and Willis D.G. 1957. The elastic coefficients of the theory of consolidation. *Journal of Applied Mechanics* 24, 594–601.

Bonnet G. 1987. Basic singular solutions for a poroelastic medium in the dynamic range. *Journal of the Acoustical Society of America* 82, 1758–1762.

Boutin C., Bonnet G. and Bard P.Y. 1987. Green's functions and associated sources in infinite and stratified poroelastic media. *Geophysical Journal of the Royal Astronomical Society* **90**, 521–550.

Burridge R. and Vargas C.A. 1979. The fundamental solution in dynamic poroelasticity. *Geophysical Journal of the Royal Astronomical Society* **58**, 61–90.

Carcione J.M. 1993. A 3-D time-domain wave equation for viscoacoustic saturated porous media. *European Journal of Mechanics A/Solids* **12**, 53–71.

Carcione J.M., Kosloff D. and Kosloff R. 1988. Wave propagation simulation in a linear viscoelastic medium. *Geophysical Journal of the Royal Astronomical Society* **95**, 597–611.

Carman P.C. 1961. L'écoulement des gaz à travers les milieux poreux. *Bibliothèques des Sciences et Techniques Nucléaires*. Presses Universitaires de France, Paris.

Dai N., Vafidis A. and Kanasewich E.R. 1995. Wave propagation in heterogeneous porous media: a velocity-stress, finite-difference method. *Geophysics*. **60**, 327–340

Deresiewicz H. and Rice J.T. 1962. The effect of boundaries on wave propagation in a liquid-filled porous solid: III. Reflection of plane waves at a free plane boundary (geneal case). *Bulletin of the Seismological Society of America* **52**, 595–625.

Dvorkin J., Nolen-Hoeksema R. and Nur A. 1994. The squirt-flow mechanism: Macroscopic description. *Geophysics* **59**, 428–438.

Garg S.K., Nayfey A.H. and Good A.J. 1974. Compressional waves in fluid-saturated elastic porous media. *Journal of Applied Physics* **45**, 1968–1974.

Geertsma J. and Smit D.C. 1961. Some aspects of elastic wave propagation in fluid-saturated porous solids. *Geophysics* **26**, 169–181.

Hassanzadeh S. 1991. Acoustic modeling in fluid-saturated porous media. *Geophysics* **56**, 424–435.

Herrera I. and Gurtin M.E. 1965. A correspondence principle for viscoelastic wave propagation. *Quarterly of Applied Mathematics* **22**, 360–364.

Kazi-Aoual M.N., Bonnet G. and Jouanna P. 1988. Green's functions in an infinite transversely isotropic saturated poroelastic medium. *Journal of the Acoustical Society of America* **84**, 1883–1889.

Lancaster P. and Tismenetsky M. 1985. *The Theory of Matrices, second edition, with Applications*. Academic Press, Inc.

Liu H.P., Anderson D.L. and Kanamori H. 1976. Velocity dispersion due to anelasticity: implications for seismology and mantle composition. *Geophysical Journal of the Royal Astronomical Society* **47**, 41–58.

Lumley D., Nur A., Dvorkin J. and Packwood J. 1994. Seismic monitoring of oil production: A feasibility study. 64th SEG meeting, Los Angeles, Expanded Abstracts, 319–322.

Mochizuki S. 1982. Attenuation in partially saturated rocks. *Journal of Geophysical Research* **87**, 8598–8604.

Murphy W.F., Winkler K.W. and Kleinberg R.L. 1986. Acoustic relaxation in sedimentary rocks: Dependence on grain contacts and fluid saturation. *Geophysics* **51**, 757–766.

Norris, A.N. 1985. Radiation from a point source and scattering theory in a fluid-saturated porous solid. *Journal of the Acoustical Society of America* **77**, 2012–2023.

Norris A.N. 1986. On the viscodynamic operator in Biot's equations of poroelasticity. *Journal of Wave-Material Interaction* **1**, 365–380.

Norris A.N. 1989. Stoneley-wave attenuation and dispersion in permeable formations. *Geophysics* **54**, 330–341.

Pilant W.L. 1979. *Elastic Waves in the Earth*. Elsevier Science Publishing Co.

Plona T.J. 1982. Acoustics of fluid-saturated porous media. Ultrasonics Symposium *IEEE* **2**, 1044–1048.

Rasolofosaon P.N.J. 1991. Plane acoustic waves in linear viscoelastic porous media: Energy, particle displacement, and physical interpretation. *Journal of the Acoustical Society of America* **89**, 1532–1550.

Sandhu R.S., Shaw H.L. and Hong S.J. 1990. A three-field finite element procedure for analysis of elastic wave propagation through fluid-saturated soils. *Soil Dynamics and Earthquake Engineering* **9**, 58–65.

Santos J.E., Corbero J. and Douglas Jr. J. 1990a. Static and dynamic behaviour of a porous solid saturated by a two-phase fluid. *Journal of the Acoustical Society of America* **87**, 1428–1438.

Santos J.E., Douglas Jr. J., Corbero J. and Lovera O.M. 1990b. A model for wave propagation in a porous medium saturated by a two-phase fluid. *Journal of the Acoustical Society of America* **87**, 1439–1448.

Schmitt, D.P., Bouchon M. and Bonnet G. 1988. Full-wave synthetic acoustic logs in radially semiinfinite saturated porous media. *Geophysics* **53**, 807–823.

Turgut A. and Yamamoto T. 1988. Synthetic seismograms for marine sediments and determination of porosity and permeability. *Geophysics* **53**, 1056–1067.

Zhu X. and McMechan G.A. 1991. Numerical simulation of seismic responses of poroelastic reservoirs using Biot theory. *Geophysics* **56**, 328–339.